Available online at www.sciencedirect.com
ScienceDirect
Trans. Nonferrous Met. Soc. China 33(2023) 1114−1123
Transactions of Nonferrous Metals Society of China
www.tnmsc.cn

Multi-scale characterizations of microstructure and mechanical properties of Ti6242 alloy linear friction welded joint with post-welded heat treatment

Zong-yu DANG[1], Guo-liang QIN[1], Hong MA[1], Pei-hao GENG[2]

1. School of Materials Science and Engineering, Shandong University, Jinan 250061, China;
2. Joining and Welding Research Institute, Osaka University, Osaka, 567-0047, Japan

Received 10 December 2021; accepted 11 May 2022

Abstract: A near α titanium alloy (Ti6242) was joined by the linear friction welding technique followed by the post-welded heat treatment (PWHT). Both joints in as-welded and PWHTed conditions were characterized in a multi-scale manner to investigate the evolution of microstructure and establish the relationship between the microstructure and mechanical properties of the joints. Results show that both joints fail in the base material, while the PWHTed joints have large hardness enhancement in the welding line (WL) and thermo-mechanically affected zone (TMAZ). After heat treatment, the cluster of the flakier α phase is formed inside the equiaxed grains in WL, while the martensite phase in TMAZ is decomposed into the (α+β) phase, both of which can improve the hardness of the joint.

Key words: linear friction welding; Ti6242; post-welded heat treatment; multi-scale characterization; microstructure; mechanical properties

1 Introduction

Linear friction welding (LFW), as a solid phase joining process, realizes the welding of two components by the oscillatory motion of one component relative to another under the action of friction pressure [1,2]. With the application of key parameters, including amplitude, frequency and friction pressure, varying heat levels can be generated at the friction interface to plasticize the material and promote the mutual diffusion of atoms of both components [3]. Therefore, LFW presents clear advantages such as high welding efficiency, and no hot crack, which has been attracted considerable attention in recent years. More importantly, under the thermo-mechanical coupling effect, the plasticized materials can be expelled from the interface, which effectively avoids the existence of oxidation and other contaminations that possibly exist at original weld interface, which is referred to as self-cleaning mechanism [4−6].

Up to now, LFW has been used to join aluminum alloy [7,8], steel [9,10], superalloy [11,12], titanium alloy (Ti alloy) [13,14] and dissimilar metals [15,16] with different levels of success. Among different materials, titanium alloy has a wide range of applications as the structural component in the aerospace field because of its low density, high strength, good corrosion and fatigue resistance [17−21]. Because of the low thermal conductivity of titanium alloys, the molten pool is susceptible to oxygen and nitrogen contamination and prone to the formation of porosity, cracks and other defects, making it of significant difficulty to obtain sound titanium alloy joint. Compared to the fusion welding technique, LFW holds obvious advantages in obtaining high-strength Ti alloy joints.

Corresponding author: Guo-liang QIN, Tel: +86-15805312185, E-mail: glqin@sdu.edu.cn
DOI: 10.1016/S1003-6326(23)66169-2

Numerous researches have been conducted on the microstructure [22], mechanical properties [23] and even simulation of different Ti alloys [14].

For the LFW of near α Ti alloys, the LFWed joint can be divided into welding line (WL), thermo-mechanically affected zone (TMAZ) and heat affected zone (HAZ). The WL is mainly recrystallized grains formed by fine martensite α' and original β phase structure. The TMAZ consists of deformed primary α, secondary α and retained β. The structure of the HAZ is similar to that of the base material (BM) [24,25]. Since WL, being the area with the highest processing temperature during welding, could reach the critical phase transition temperature, a high fraction of α phase can be observed in WL with almost no β phase [26]. Due to grain refinement in the WL and work hardening in TMAZ, the welded area usually showed higher strength than BM, leading to the fracture at BM [18,25,26]. As for the microhardness of the welded joints, different researchers have come to different conclusions. Some researchers have shown that the microhardness gradually increases from BM to WL and reaches the maximum at the WL [18,24,26]. However, RAJAN et al [25] reported that there would be a distinct softening area in the HAZ of the joint. GUO et al [27] found that the HAZ and WL had a lower microhardness than the base metal, which was related to the transformation of the β to orthorhombic α'' during the welding process. Fewer studies have been conducted on other aspects of the mechanical properties of near α titanium alloy LFWed joints such as the variation of local modulus and strength, which needs to be further studied.

The post-welded heat treatment (PWHT) of titanium alloys is an important means of tuning the properties of welded joints. Since near α titanium alloys are not heat-treatable strengthened titanium alloys, the role of heat treatment after LFW is mainly to reduce the possible residual stress generated during the welding process. FRANKEL et al [28] reported that the residual stresses on the Ti6242 side are significantly reduced after the PWHT of the dissimilar titanium alloy LFWed joint. However, MESHRAM and MOHANDAS [29] found that PWHT at 700 ℃ for 2 h would damage the ductility of the joint, which was relevant to the precipitation of silicide. Different results in the above literatures may be due to the different temperatures employed in their studies, causing distinct annealing behavior of the joint. Hence, more studies are required to clarify the above explanations.

In this work, for LFWed joints of near α titanium alloy, Ti6242, multi-scale characterizations of microstructure evolution, grain orientation and texture in different regions of the joints by using a scanning electron microscope (SEM) and electron backscattered diffraction (EBSD), and multi-technics characterization of mechanical properties of the joints by using digital image correlation (DIC) and nanoindentation techniques were conducted to get an in-depth understanding of the microstructure evolution and mechanical performance of the joint with/without heat treatment. Moreover, the local bonding strength of as-welded and PWHTed joints in different characteristic zones was revealed.

2 Experimental

2.1 Material and welding process

The material used in the present experiment was Ti6242, the near α titanium alloy, with the chemical composition measured by optical emission spectrometer (M12, Spectro-Lab) as given in Table 1. Blocks of 8 mm × 16 mm × 35 mm were cut by electronic discharge machining (EDM) from a Ti6242 forged billet, while the area of 8 mm × 16 mm was the friction interface with the oscillation direction being along the y-axis and the forging direction along the z-axis, as shown in Fig. 1(a).

Table 1 Main chemical composition of Ti6242 alloy (wt.%)

Al	Sn	Zr	Mo	Si	Ti
6.17	2.03	4.08	1.96	0.075	Bal.

The LFW equipment used was an HSMZ-30 developed by Harbin Welding Institute Limited Company. The controlled welding parameters of LFW were frequency (f), amplitude (A), friction pressure (P) and friction time (t). Prior to welding, the faying surfaces were ground by sandpaper and wiped with alcohol to remove grease and oxide. Based on a preliminary study, welding was applied at the welding condition of f=20 HZ, A=3 mm, P=100 MPa and t=3 s. The welding process is

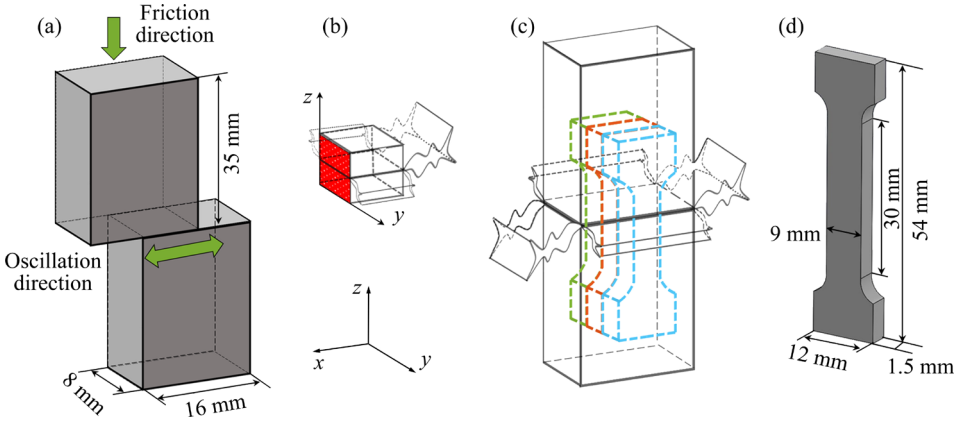

Fig. 1 Schematic diagram of welding process and specimen dimensions (a), sampling position of metallographic specimens (b), sampling position of tensile specimens (c), and dimensions of tensile specimens (d)

displayed in Fig. 1(a). The average burn-off was 7.3 mm. The welded joint was then subjected to a PWHT process at 595 °C for 8 h and then air-cooled to room temperature.

2.2 Experimental procedures

Metallographic specimens were cut by an EDM in a direction perpendicular to the friction interface, which is shown schematically in Fig. 1(b). After that, the samples were ground with sand-paper with different grits and polished with 0.5 μm diamond paste. Specimens dedicated to macro-appearance and microstructure inspection were analyzed by the optical microscope (ECLIPSE LV150N, Zeiss) and the field emission SEM (JSM-7800F) using the backscatter electrons (BSE) detector after being etched with the Keller's reagent (2.5 mL HNO_3 + 1.5 mL HCl + 1 mL HF + 95 mL H_2O). The texture orientation and grain size at different positions of the welded joint were characterized by EBSD (NordlysMax3, Oxford) equipped on the above-mentioned SEM. EBSD specimens were prepared by electrolytic polishing (voltage: 35 V, time: 10 s, temperature: 0 ℃) in a mixture of 10 mL perchloric acid and 200 mL alcohol.

For characterization of mechanical properties, a universal tensile machine, equipped with a DIC system, with a tensile rate of 1 mm/min was used to measure the tensile strength of the welded joints in a displacement-controlled mode. The detailed sampling position and dimensions of the tensile specimens are shown in Figs. 1(c, d). Microhardness was measured by a microhardness tester (HXD-1000C) with a load of 500 g for dwell time of 10 s across the welding line zone. Nanoindentation (HYSITRON TI 980) with Berkovich tip was used to explore further the properties of different phases in the characteristic regions.

3 Results and discussion

3.1 Microstructure of base material

Figure 2(a) shows the microstructure of Ti6242 alloy base material, from which it can be seen that the BM contains the dark-colored primary α phase and the light-colored retained β phase. There are two kinds of α phase: the one existing along the β grain boundary is called grain boundary α, and the other located inside the original β phase is called basket-weave α [27].

3.2 Microstructure of as-welded and PWHTed joints

The macrostructure of the as-welded joint from the welding interface to BM is shown in Fig. 3. The whole LFWed joint has no obvious welding defects, such as pores and cracks. The welded joint can be divided into the WL and TMAZ with no obvious HAZ observed. The microstructure of the WL is significantly different from the other zones, characterized by fine equiaxed grains. The formation of such grain is attributed to the higher temperature at the friction interface enabling the subsequent recrystallization. TMAZ is subjected to severe plastic deformation and its grains are deformed. The shape and distribution of α grains are elongated along the direction of deformation. On account of the low-temperature joining feature of LFW, it is difficult to distinguish the HAZ. The

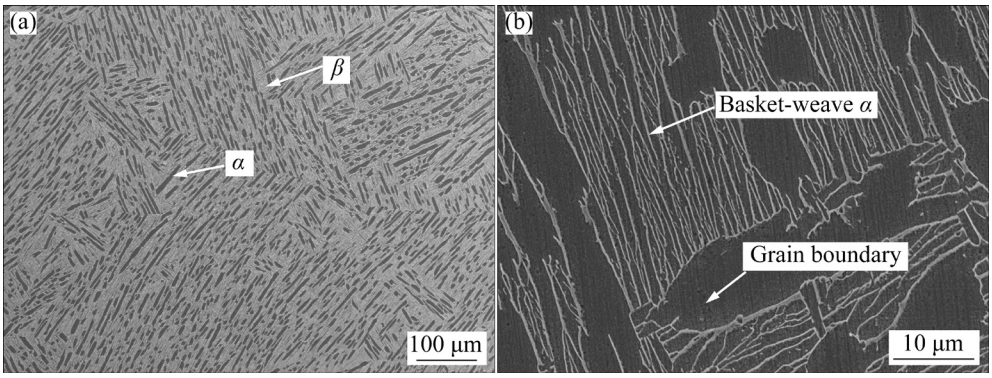

Fig. 2 Microstructure of Ti6242

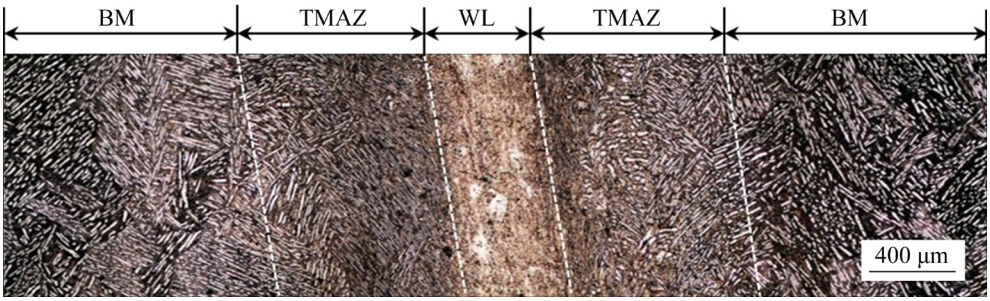

Fig. 3 Metallographic image of different zones of as-welded joints

previous literature has shown that the microstructure difference between HAZ and BM was the grain size as no significant heat and force were experienced in HAZ [30]. Therefore, the further characterization of HAZ was not performed. In order to further investigate the microstructure in different regions, SEM analysis was conducted.

The typical microstructure at different zones of the as-welded and PWHTed joints using SEM is shown in Fig. 4. The temperature in the WL exceeds the β transformation temperature of the titanium alloy, leading to the phase transformation of α to β. Due to large cooling rate after welding, the β phase cannot be completely transformed to the α phase. Therefore, only a small amount of flaky α phase is precipitated along the grain boundary to form a rim. As the temperature continuously drops, the flaky α phase can also be formed inside the grain, as shown in Fig. 4(a). After PWHT, more flakier α phases precipitate and clusters are formed in the equiaxed grains in Fig. 4(d). A different microstructure is also observed at the TMAZ. The most significant feature in the as-welded joint is the growth of the β phase and the wave-shape of both phases under the action of plastic deformation at a lower temperature in comparison with WL. The α' martensite also exists in TMAZ. Through PWHT, fine needle-like phases (α+β) appear on the β phase, making the boundary between α and β phase blurred. This is mainly due to the fact that the martensite α' generated at TMAZ is a typical metastable phase. Upon heating, the decomposition of α' to α occurs, leading to the growth of needle-like phases. The BM subjected to PWHT has fine-sized spherical secondary phases formed, where the Si and Zr elements aggregate on the lamellae during the heating process [31].

3.3 Texture characteristics of as-welded and PWHTed joints

The evolution of the microstructure during LFW has a great impact on the texture, which also affects the mechanical properties of joints [32,33]. Therefore, the pole figures of α phase at different regions in the as-welded and PWHTed joints are shown in Fig. 5. Due to the presence of a large number of α phase stabilizing elements in Ti6242 alloy, the BM contains a very small amount of β phase. In the as-welded and PWHTed joints, the texture density at the same regions is relatively close and the type of texture is similar. Interestingly, a high texture density as well as several typical

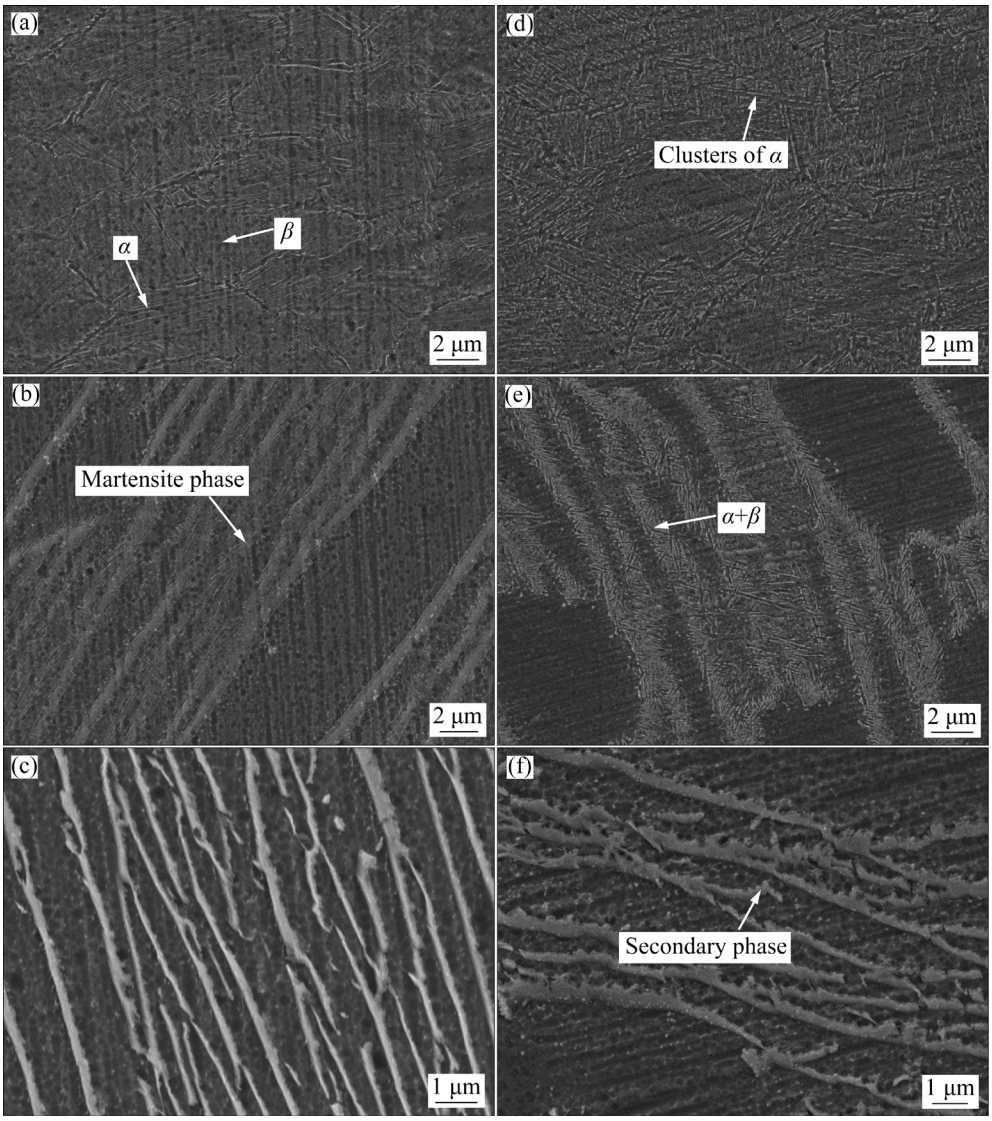

Fig. 4 Microstructures of different regions of as-welded (a, b, c) and PWHTed (d, e, f) joints: (a, d) WL; (b, e) TMAZ; (c, f) BM

textures are present in the BM, as shown in the {1000} pole diagrams of Figs. 5(a, d). This is mainly related to the EBSD scanning area, where the large grains in the BM make the acquisition area contain only a few grains. Therefore, the density of the texture is larger at both BM and TMAZ. Because dynamic recrystallization occurs in the WL leading to finer grain sizes, the texture density is reduced to some extent. This phenomenon was also reported in the study of WANG et al [34].

Four different types of textures are mainly shown in Fig. 5, which are transverse (T) texture ($\{10\bar{1}0\}\langle 11\bar{2}0\rangle$), basal (B) texture, rolling (R) texture ($\{11\bar{2}2\}\langle 11\bar{2}3\rangle$) and R1 texture. These textures have been confirmed in previous studies [32]. The B texture is present in different regions of both joints. The BM of Ti6242 has a stronger B texture and the weaker R and R1 texture. After heat treatment, there is almost no change in the texture of the BM. In the as-welded joint, TMAZ has a stronger B texture, while the T texture replaces the R and R1 texture in BM, being the only one remaining among the 12 possible variants. As for the WL, B texture becomes weaker, while a stronger R texture reappears. The texture change in titanium alloy is directly related to phase transition between α and β phases (about 1007 °C) [35]. The T texture formed at TMAZ is most likely due to the formation of the martensite in the TMAZ that hinders the selection of other variants [36,37]. The dynamic recrystallisation in WL may promote the reappearance of R texture. However, the texture

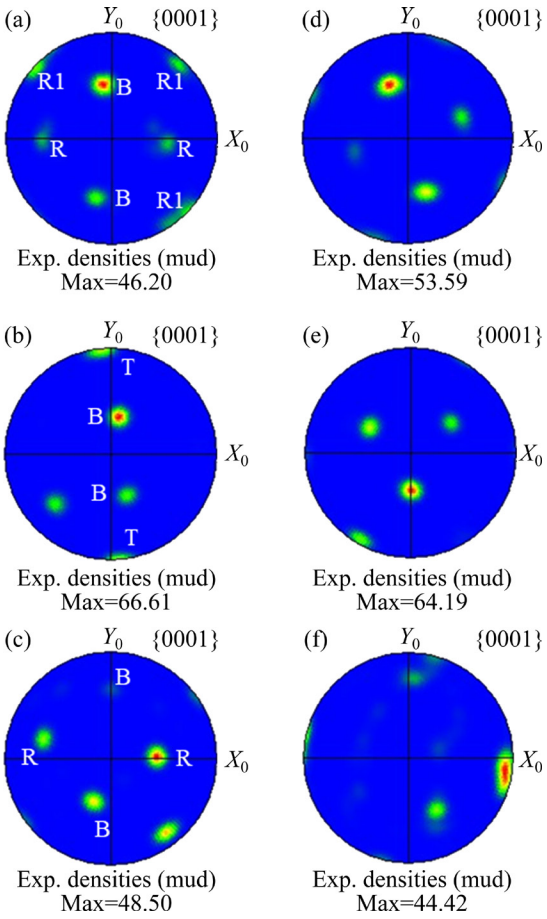

Fig. 5 Polar figures of α phase in different regions of as-welded (a, b, c) and PWHTed (d, e, f) joints: (a, d) BM; (b, e) TMAZ; (c, f) WL (X_0 is pressure direction, and Y_0 is oscillation direction)

at TMAZ and WL of PWHTed joints is changed. The intensity distribution in the polar diagram is not regular, which means that different types of texture may have been generated, as shown in Figs. 5(e, f). This could be attributed to the microstructure changes that occur after PWHT as observed above. In particular, the sub-stable martensite decomposes into (α+β) phases, resulting in a more deviant texture pattern in the pole figure in Fig. 5(e).

3.4 Mechanical properties of as-welded and PWHTed joints

3.4.1 Microhardness and nanoindentation test results

Microhardness tests are performed on the center of the metallographic specimens along the direction perpendicular to the WL with the results shown in Fig. 6. The hardness value of the welded joint is symmetrically distributed about the WL. The lowest hardness of the BM is about HV 330, while in the TMAZ and WL, the hardness value rises significantly and reaches the maximum value (about HV 400) at the WL. This trend is consistent with the previously-reported one in LFWed Ti alloys [24,34,38,39]. For the PWHTed joint, the hardness of both WL and TMAZ increases and the highest value can reach up to about HV 430 at WL, still being the area with the highest hardness in the whole joint, but the hardness of the BM is not changed significantly. The α phase is gradually precipitated inside the equiaxed grains at the WL after heat treatment and a cluster of α phase is formed. Although a certain amount of martensite α' is formed at the welded joint, it has little effect on the microhardness of the joint. The martensite α' formed in the β phase in TMAZ is sub-stable and decomposes into fine (α+β) phases after heat treatment. Both of these play a significant role in the increase of the microhardness of welded joints.

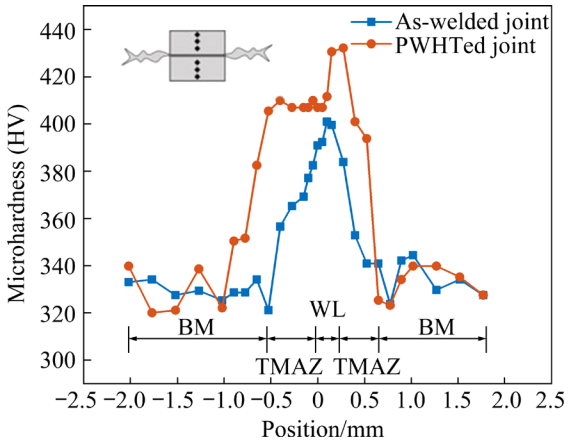

Fig. 6 Microhardness curves of as-welded and PWHTed joints

The microhardness of the different regions of the joint in the two states shows a large difference and it fails to reveal the subtle variations of the joint following PWHT due to relatively large indenter, so nanoindentation tests are conducted for the larger size α phase in titanium alloy to investigate the variation of the hardness and elastic modulus of α phase in different regions. Figure 7 shows the load−indentation depth curves for the α phase of the two joints obtained from the nanoindentation test. Table 2 gives the nanoindentation hardness values and elastic modulus values of the α phase at different regions. The hardness and elastic modulus of the α phase in BM are close to those in TMAZ of the as-welded joint. After heat treatment, the

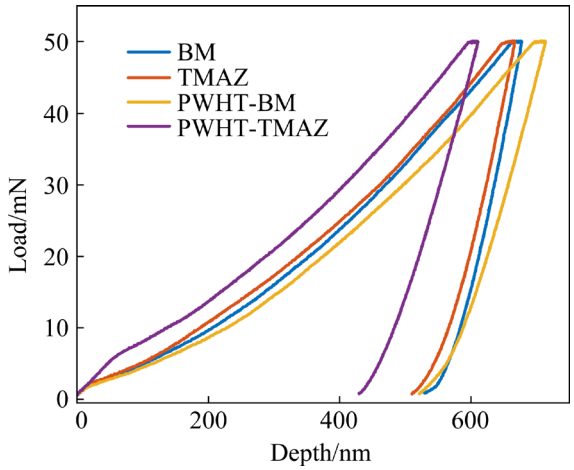

Fig. 7 Load−depth curves of α phase in BM and TMAZ in as-welded and PWHTed joints

Table 2 Nanoindentation hardness and elastic modulus values of α phase

Region	Hardness/GPa	Elastic modulus/GPa
BM	5.2	149.7
TMAZ	5.4	147.5
PWHT-BM	5.1	106.5
PWHT-TMAZ	6.8	119.4

hardness of the α phase in the BM (maximum indentation depth of ~610 nm) is not changed much, while the hardness value of the α phase in the TMAZ (~508 nm) increases significantly from 5.38 to 6.75 GPa. This is related to the microstructural transformation after heat treatment.

3.4.2 Tensile behavior and fracture morphology

The influence of different microstructures on the tensile property of as-welded and PWHTed joints is explored. The DIC device is able to obtain macroscopic engineering stress and strain curves and strain accumulation maps for both joints. Figures 8(a, c) show the macroscopic engineering stress−strain curves for the tensile process of the as-welded and PWHTed joints. The accumulated strain maps at five different moments on the curve are extracted, as shown in Figs. 8(b, d). It is found that the fracture location of both joints is far from the WL and the strength of the joint is improved after heat treatment. However, the engineering strain in the tensile test of the PWHTed joint is significantly reduced to half that of as-welded joint (from 4.9% to 2.5%), indicating that the ductility of the PWHTed joint is severely damaged. The cumulated local strain field (ε_{pp}) maps in Fig. 8(b)

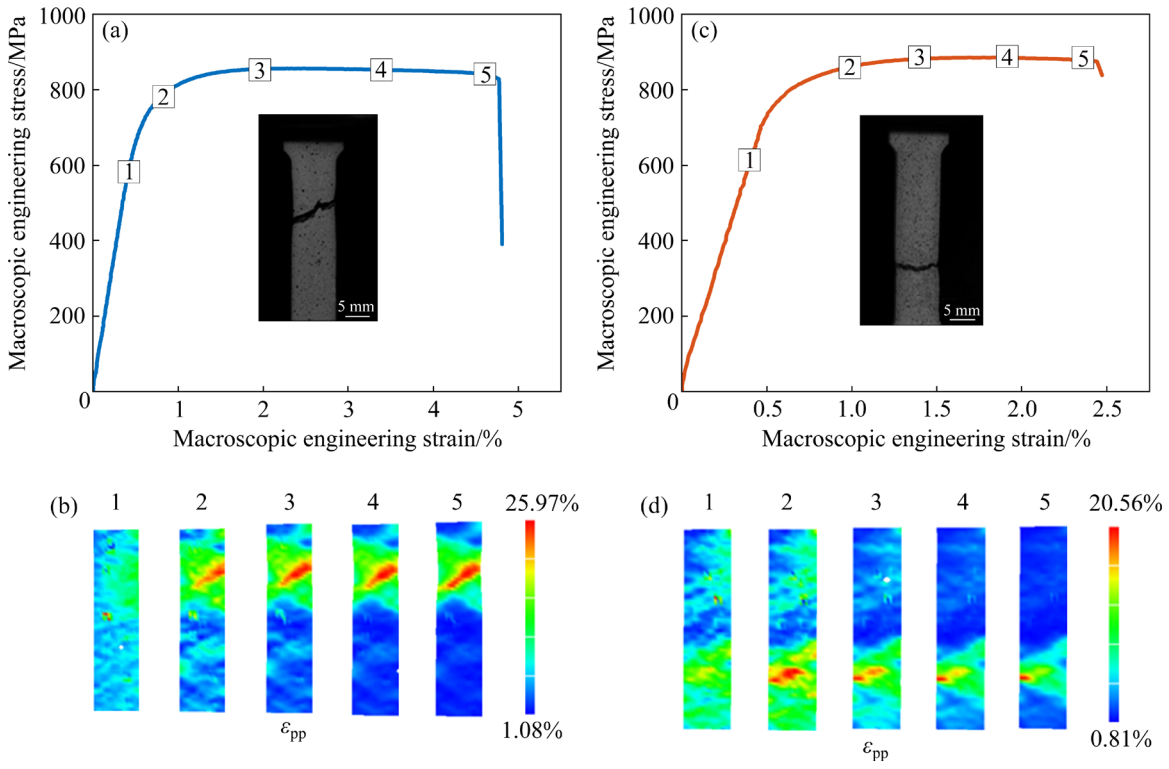

Fig. 8 Results for DIC tensile tests: (a, b) Stress−strain diagrams and ε_{pp} cumulated strain fields for tensile testing of as-welded joints; (c, d) Stress−strain diagrams and ε_{pp} cumulated strain fields for tensile testing of PWHTed joints

show that the ε_{pp} distribution on the whole tensile specimen is more uniform when the load is applied at the initial stage. With further loading, the ε_{pp} fields become non-uniform. A noticeable increase at a certain location in the BM affects the surrounding area over a wide range. The ε_{pp} field at failure is 25.97% and the fracture is in a shear mode with 45° to the loading direction. In contrast, the ε_{pp} fields at failure for the PWHTed joint are only 20.56%, but the range of the ε_{pp} fields is more concentrated. This phenomenon demonstrates that following the heat treatment, the strength of WL and TMAZ is preserved, being higher than that of the base metal regardless of the heat treatment state, whereas it possesses a significant effect on the strength and ductility of the BM.

The results of tensile strengths are given in Table 3. The BM tensile tests show that the mean ultimate tensile strength (UTS) is 867 MPa, while UTS of BM increases to 882.4 MPa after PWHT. It is generally believed that the strength in the WL region is due to the recrystallization of the welding process forming fine equiaxed grains. And the faster cooling rate after welding makes it difficult for the fine grains to grow, thus forming a fine grain strengthening effect. For TMAZ, the work hardening due to severe plastic deformation increases the strength in this region compared to the BM. The increase in tensile strength of the BM after heat treatment can be attributed to the strengthening effect of the spherical second phase particles precipitated.

Table 3 Results of tensile strength for different joints (MPa)

As-welded	PWHT	BM	PWHT-BM
841.7±17.32	857.7±19.16	867.0±5.55	882.4±12.04

Figure 9 shows the fracture morphologies of the as-welded and PWHTed joints. The fracture type of both joints is the ductile−brittle fracture where tear edges and dimples are presented. But the fracture surface in the as-welded joint consists of more uniform and deep dimples, which indicates higher ductility. This is consistent with the results of the DIC tensile analysis and nanoindentation tests.

4 Conclusions

(1) A sound LFWed joint of Ti6242 alloy is obtained. The WL in the as-welded joint is composed of equiaxed recrystallized grains, while a cluster of lamellar α phase is distributed in the equiaxed grains after PWHT. The TMAZ is subjected to severe plastic deformation with the deformed α phase and a certain amount of α' martensitic phase is formed. After PWHT, the α' martensitic phase transforms into (α+β) phase.

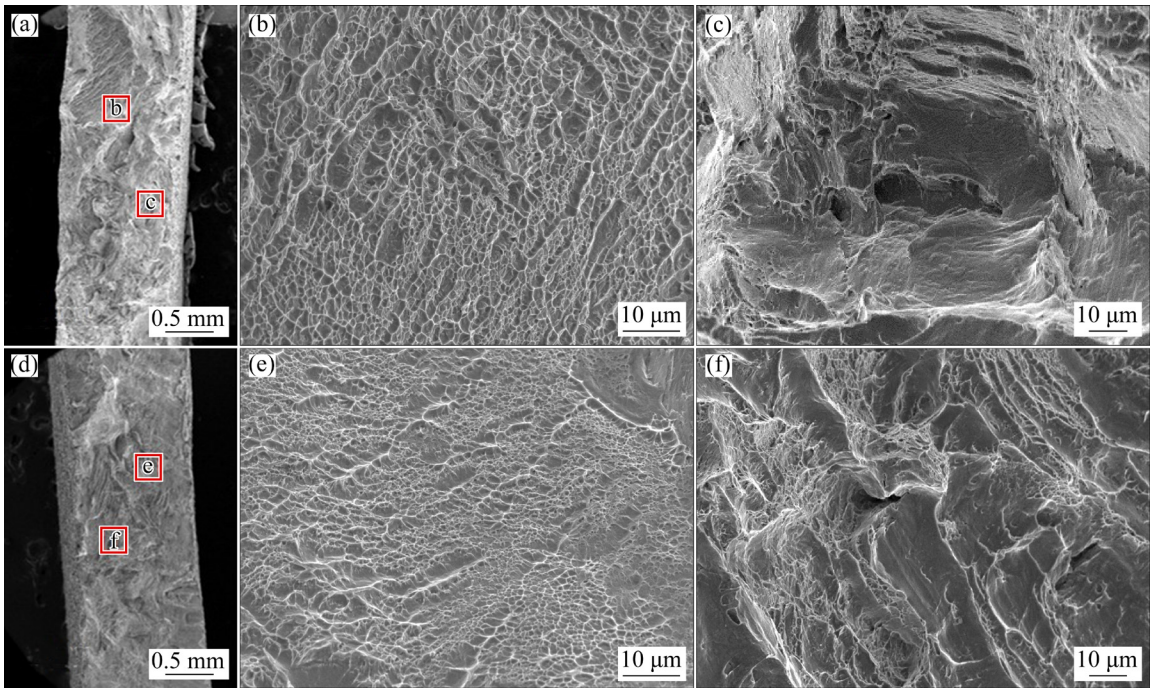

Fig. 9 Fracture morphologies of as-welded (a−c) and PWHTed (d−f) joints

There is no obvious change in the BM except the precipitation of a small amount of spherical second phase.

(2) B, T, R and R1 textures are found to exist in the LFWed joint. B texture exists in different regions of the joints with or without heat treatment. The transformation of R and R1 texture to T texture in TMAZ of the as-welded joint may be related to the generation of the martensite, which hinders the nucleation of other texture variants. However, the TMAZ in the PWHTed joint is shown to have other different types of texture due to the decomposition of martensite.

(3) The microhardness of the WL and TMAZ is higher in the PWHTed joints compared to that of similar regions in the as-welded joints, while the hardness has no significant changes in the BM. After tensile tests, the fracture of both as-welded and PWHTed joints is located in the BM, but the latter shows higher tensile strength and reduced ductility, which may be attributed to the precipitation of the second phase of the BM.

Acknowledgments

This study was supported by the National Natural Science Foundation of China (No. 52005294). The first author would also thank Mr. Jun ZHOU, Mr. Liang WU and Mr. Rui LI from Harbin Welding Institute Limited Company for their support of the welding experiment.

References

[1] MCANDREW A R, COLEGROVE P A, BÜHR C, FLIPO B C, VAIRIS A. A literature review of Ti−6Al−4V linear friction welding [J]. Progress in Materials Science, 2018, 92: 225−257.

[2] UDAY M B, FAUZI M N, ZUHAILAWATI H, ISMAIL A B. Advances in friction welding process: A review [J]. Science and Technology of Welding and Joining, 2010, 15(7): 534−558.

[3] BOYAT X, BALLAT-DURAND D, MARTEAU J, BOUVIER S, FAVERGEON J, OREKHOV A, SCHRYVERS D. Interfacial characteristics and cohesion mechanisms of linear friction welded dissimilar titanium alloys: Ti−5Al−2Sn−2Zr−4Mo−4Cr (Ti17) and Ti−6Al−2Sn−4Zr−2Mo (Ti6242) [J]. Materials Characterization, 2019, 158: 109942.

[4] GARCÍA J M, ESIN V A, MORGENEYER T F. Strength, fatigue strength and toughness of dissimilar Ti17–Ti64 linear friction welded joints: Effect of soft surface contamination and depletion of α precipitates [J]. Materials Science and Engineering A, 2021, 799: 139989.

[5] WANG X Y, LI W Y, YE Q, YANG X W, MA T J, VAIRIS A. Linear friction welding of a beta titanium alloy: Experimental investigations on microstructure evolution and mechanical properties [J]. Science and Technology of Welding and Joining, 2020, 25(8): 625−636.

[6] CHAMANFAR A, JAHAZI M, CORMIER J. A review on inertia and linear friction welding of Ni-based superalloys [J]. Metallurgical and Materials Transactions A: Physical Metallurgy and Materials Science, 2015, 46(4): 1639−1669.

[7] BUFFA G, CAMMALLERI M, CAMPANELLA D, COMMARE U L, FRATINI L. Linear friction welding of dissimilar AA6082 and AA2011 aluminum alloys: Microstructural characterization and design guidelines [J]. International Journal of Material Forming, 2017, 10(3): 307−315.

[8] BUFFA G, CAMMALLERI M, CAMPANELLA D, FRATINI L. Shear coefficient determination in linear friction welding of aluminum alloys [J]. Materials & Design, 2015, 82: 238−246.

[9] LI Y M, LIU Y C, LIU C X, LI C, MA Z Q, HUANG Y, WANG Z M, LI W Y. Microstructure evolution and mechanical properties of linear friction welded S31042 heat-resistant steel [J]. Journal of Materials Science & Technology, 2018, 34(4): 653−659.

[10] LIU C X, GAO Y, LI X H, LI W C, GAN K F. Study on microstructure and mechanical property of linear friction welding on 9Cr reduced activation ferrite/martensite steel [J]. Journal of Nuclear Materials, 2020, 531: 152011.

[11] YANG X W, LI W Y, LI J L, XIAO B, MA T J, HUANG Z, GUO J. Finite element modeling of the linear friction welding of GH4169 superalloy [J]. Materials & Design, 2015, 87: 215−230.

[12] GENG P H, QIN G L, LI T Y, ZHOU J, ZOU Z D, YANG F. Microstructural characterization and mechanical property of GH4169 superalloy joints obtained by linear friction welding [J]. Journal of Manufacturing Processes, 2019, 45: 100−114.

[13] MA T J, LI W Y, YANG S Y. Impact toughness and fracture analysis of linear friction welded Ti−6Al−4V alloy joints [J]. Materials & Design, 2009, 30: 2128−2132.

[14] LI W Y, MA T J, LI J L. Numerical simulation of linear friction welding of titanium alloy: Effects of processing parameters [J]. Materials & Design, 2010, 31: 1497−1507.

[15] JIAO Z, SONG C B, LIN T S, HE P. Molecular dynamics simulation of the effect of surface roughness and pore on linear friction welding between Ni and Al [J]. Computational Materials Science, 2011, 50(12): 3385−3389.

[16] WANJARA P, DALGAARD E, TRIGO G, MANDACHE C, COMEAU G, JONAS J J. Linear friction welding of Al−Cu: Part 1 — Process evaluation [J]. Canadian Metallurgical Quarterly, 2011, 50(4): 350−359.

[17] GARCÍA J M, GASLAIN F, MORGENEYER T F. On the effect of a thermal treatment on the tensile and fatigue properties of weak zones of similar Ti17 linear friction welded joints and parent material [J]. Materials Characterization, 2020, 169: 110570.

[18] GARCÍA J M, MORGENEYER T F. Strength and fatigue strength of a similar Ti−6Al−2Sn−4Zr−2Mo−0.1Si linear friction welded joint [J]. Fatigue & Fracture of Engineering Materials & Structures, 2019, 42(5): 1100−1117.

[19] XU J W, ZENG W D, ZHOU D D, HE S T, JIA R C. Evolution of coordination between α and β phases for two-phase titanium alloy during hot working [J]. Transactions of Nonferrous Metals Society of China, 2021, 31(11): 3428−3438.

[20] CHEN Y, XU W C, SHAN D B, GUO B. Microstructure evolution of TA15 titanium alloy during hot power spinning [J]. Transactions of Nonferrous Metals Society of China,

2011, 21(S2): s323−s327.
[21] SUN H, YU L M, LIU Y C, ZHANG L Y, LIU C X, LI H J, WU J F. Effect of heat treatment processing on microstructure and tensile properties of Ti−6Al−4V−10Nb alloy [J]. Transactions of Nonferrous Metals Society of China, 2019, 29(1): 59−66.
[22] WANG X Y, LI W Y, MA T J, VAIRIS A. Characterisation studies of linear friction welded titanium joints [J]. Materials & Design, 2017, 116: 115−126.
[23] WANJARA P, JAHAZI M. Linear friction welding of Ti−6Al−4V: Processing, microstructure, and mechanical-property inter-relationships [J]. Metallurgical and Materials Transactions A: Physical Metallurgy and Materials Science, 2005, 36(8): 2149−2164.
[24] BALLAT-DURAND D, BOUVIER S, RISBET M, PANTLEON W. Through analysis of the microstructure changes during linear friction welding of the near-α titanium alloy Ti−6Al−2Sn−4Zr−2Mo (Ti6242) towards micro-structure optimization [J]. Materials Characterization, 2019, 151: 38−52.
[25] RAJAN S, WANJARA P, GHOLIPOUR J, KABIR A S. Microstructure, tensile properties, and fatigue behavior of linear friction-welded Ti−6Al−2Sn−4Zr−2Mo−0.1Si [J]. Materials, 2021, 14(1): 30.
[26] SU Y, LI W Y, WANG X Y, MA T J, YANG X W, VAIRIS A. On microstructure and property differences in a linear friction welded near-alpha titanium alloy joint [J]. Journal of Manufacturing Processes, 2018, 36: 255−263.
[27] GUO Y, JUNG T, CHIU Y L, LI H Y, BRAY S, BOWEN P. Microstructure and microhardness of Ti6246 linear friction weld [J]. Materials Science and Engineering A, 2013, 562: 17−24.
[28] FRANKEL P, PREUSS M, STEUWER A, WITHERS P J, BRAY S. Comparison of residual stresses in Ti−6Al−4V and Ti−6Al−2Sn−4Zr−2Mo linear friction welds [J]. Materials Science and Technology, 2009, 25(5): 640−650.
[29] MESHRAM S D, MOHANDAS T. Influence of matrix microstructure on aging response of near alpha titanium alloy (IMI834) parent metal and welds on toughness [J]. Materials Science and Technology. 2011, 27(1): 235−239.
[30] WANG X Y, LI W Y, MA T J, YANG X W, VAIRIS A. Microstructural evolution and mechanical properties of a linear friction welded two-phase Ti−6.5Al−3.5Mo−1.5Zr−0.3Si titanium alloy joint [J]. Materials Science and Engineering A, 2019, 743: 12−23.
[31] ZHANG Jing, ZHANG Tian-cang, LI Ju. Study on microstructure and microhardness of linear friction welded joints of TA19 titanium alloy [J]. Hot Working Technology, 2017, 46(17): 59−63.
[32] KARADGE M, PREUSS M, LOVELL C, WITHERS P J, BRAY S. Texture development in Ti−6Al−4V linear friction welds [J]. Materials Science and Engineering A, 2007, 459: 182−191.
[33] BACHE M R, EVANS W J, VOICE W. The resistance to impact damage and subsequent fatigue response of two titanium alloys [J]. Materials Science and Engineering A, 2002, 333: 287−294.
[34] WANG X Y, LI W Y, MA T J, YANG X W, VAIRIS A, TAO J. Microstructural heredity and its effect on mechanical properties of linear friction welded Ti−6.5Al−3.5Mo−1.5Zr−0.3Si alloy joints [J]. Materials Characterization, 2020, 168: 110540.
[35] OBASI G C, BIROSCA S, QUINTA DA FONSECA J, PREUSS M. Effect of β grain growth on variant selection and texture memory effect during $\alpha\rightarrow\beta\rightarrow\alpha$ phase transformation in Ti−6Al−4V [J]. Acta Materialia, 2012, 60: 1048−1058.
[36] BELADI H, CHAO Q, ROHRER G S. Variant selection and intervariant crystallographic planes distribution in martensite in a Ti−6Al−4V alloy [J]. Acta Materialia, 2014, 80: 478−489.
[37] LÜTJERING G. Influence of processing on microstructure and mechanical properties of (α+β) titanium alloys [J]. Materials Science and Engineering A, 1998, 243: 32−45.
[38] WANG X Y, LI W Y, MA T J, YANG X W, VAIRIS A. Effect of welding parameters on the microstructure and mechanical properties of linear friction welded Ti−6.5Al−3.5Mo−1.5Zr−0.3Si joints [J]. Journal of Manufacturing Processes, 2019, 46: 100−108.
[39] MA T J, ZHONG B, LI W Y, ZHANG Y, YANG S Q, YANG C L. On microstructure and mechanical properties of linear friction welded dissimilar Ti−6Al−4V and Ti−6.5Al−3.5Mo−1.5Zr−0.3Si joint [J]. Science and Technology of Welding and Joining, 2013, 17(1): 9−12.

Ti6242 合金线性摩擦焊及焊后热处理接头显微组织与力学性能的多尺度表征

党宗彧[1]，秦国梁[1]，马 宏[1]，耿培皓[2]

1. 山东大学 材料科学与工程学院，济南 250061；

2. Joining and Welding Research Institute, Osaka University, Osaka, 567-0047, Japan

摘 要：通过线性摩擦焊技术对一种近 α 钛合金(Ti6242)进行连接，并进行焊后热处理。为了研究显微组织演变并建立显微组织与接头力学性能的关系，对焊态与焊后热处理的两种接头进行多尺度表征。结果表明，两种接头的断裂位置均位于母材，而经焊后热处理的接头在焊缝与热力影响区的硬度进一步提升。经过热处理后焊缝处的等轴晶粒中产生薄片状的 α 相集束，而热力影响区处的马氏体相分解为(α+β)相，从而提高焊接接头处的硬度。

关键词：线性摩擦焊；Ti6242；焊后热处理；多尺度表征；显微组织；力学性能

(Edited by Bing YANG)